BIOCHEMISTRY
including biophysical chemistry & molecular biology

Article

pubs.acs.org/biochemistry

Structural and Functional Analysis of the Transmembrane Segment Pair VI and VII of the NHE1 Isoform of the Na^+/H^+ Exchanger

Claudia Alves, Brian L. Lee, Brian D. Sykes, and Larry Fliegel*

Department of Biochemistry, University of Alberta, Edmonton, Alberta, Canada T6G 2H7

Supporting Information

ABSTRACT: Isoform 1 of the mammalian Na^+/H^+ exchanger (NHE1) is a ubiquitously expressed plasma membrane pH regulatory protein. It removes one intracellular H^+ in exchange for one extracellular Na^+. The 500 N-terminal amino acids comprise the catalytic membrane domain and fold into 12 transmembrane (TM) segments. To gain insight into the structure and function of human NHE1, a region spanning transmembrane domains VI and VII was expressed and purified, and the structure was determined using nuclear magnetic resonance (NMR). Segment VI includes two structurally conserved regions corresponding to two short α-helices involving residues 229−236 and 239−247. Segment VII includes one long helical region spanning residues 255−274. The NMR structure of the peptide containing transmembrane domains VI and VII was very similar to the previously published structures of the single-transmembrane segments except that TM VII was not kinked. Tryptophan scanning site-directed mutagenesis of TM VI demonstrated that mutation of residues V240−V245 to tryptophan eliminated NHE1 activity when the full length protein was expressed in cells. In contrast, mutants F246W and E247W were functional. Double mutant V242F/F260V retained activity, while the individual mutations were not active. The results suggest that the region of TM VI from V240 to V245 is closely associated with TM VII and that, in agreement with the NMR structure of VI−VII segments, V242 and F260 are in close association. A study of two transmembrane peptides provides further insight into the structure of the NHE1 protein.

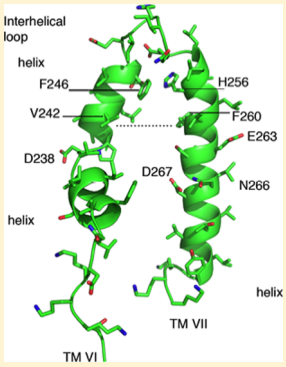

The type I isoform of the Na^+/H^+ exchanger (NHE1) is a key pH regulatory protein in mammalian cells. This isoform is ubiquitous and functions in the plasma membrane to catalyze removal of one intracellular proton in exchange for one extracellular sodium ion.[1−3] NHE1 has numerous other indirect physiological roles that accompany or are a result of its pH regulatory function. By its activation and by elevating the intracellular pH (pH_i), it promotes cell growth and differentiation.[4] Additionally, its activation facilitates inward sodium flux in response to osmotic shrinkage,[5] and it also enhances cell motility.[6] NHE1 activation enhances invasion by breast cancer cells by increasing pH_i and by acidification of the extracellular microenvironment of tumor cells.[7−11] The NHE1 isoform is present in the myocardium,[12] and elevated NHE1 activity promotes heart hypertrophy[13] and exaggerates the damage that occurs during myocardial ischemia and reperfusion. NHE1 inhibitors have been promising in preclinical trials, protecting the myocardium from various diseases.[14,15] However, clinical trials with NHE1 inhibitors are largely unfruitful, possibly because of a lack of inhibitor specificity.[16] Improved knowledge of the structure of NHE1 may facilitate the development of improved inhibitors for clinical use.

The 500 N-terminal amino acids of the mammalian NHE1 protein consist of 12 transmembrane (TM) segments that comprise the catalytic component. Two general models of the topology of NHE1 exist. One model is based on cysteine accessibility studies,[17] while the second is based on computational comparison with the suggested crystal structure of the *Escherichia coli* Na^+/H^+ exchanger NhaA[18] (these were reviewed by Kemp et al.[19]). The models vary from one another after amino acid 315. However, prior to this region, the models are essentially identical with the exception of the latter model predicting that the first two transmembrane segments are cleaved free of the protein. Amino acids 226−275 are predicted to form two transmembrane segments by hydropathy[17] analysis and in both models.

Expression and purification of entire membrane domains of eukaryotic proteins have proven to be problematic goals. However, studies have demonstrated that single-TM segments possess much of the required structural information needed to form their higher-order structures.[20−22] To gain insight into the structure and function of NHE1, we previously expressed and determined structures of single-TM segments of NHE1, including TM VI and TM VII, using nuclear magnetic resonance (NMR) spectroscopy and studied these TM segments by mutagenesis in the intact full length protein. For TM VI, our studies showed that it is a pore-lining TM segment that has a helical region, followed by an unwound region, followed by another helical region.[23,24] Our studies of TM VII demonstrated that it was predominantly α-helical, that it was critical to NHE1 function, and that it also contains pore-lining residues.[25,26]

Received: March 31, 2014
Revised: May 12, 2014
Published: May 19, 2014

While much of the required structural information is contained within the primary amino acid sequence of TM segments, interactions between TM segments can obviously not be studied with single-TM segments. Additionally, Hunt et al.[21] have suggested that in some cases, the interactions between helices and the presence or absence of the interhelical loops can affect the conformation of TM segments. While examining TM segments representing fragments of bacteriorhodopsin, they found that in five of seven cases the polypeptides formed stable TM segments representing the native protein. However, in two cases, the TM segments formed non-native configurations. A lack of links between helices was one putative explanation for the aberrant structures. For this reason, we examined a pair of TM segments, TM VI and TM VII, that are linked together by a short intracellular loop. We developed a system to express and purify the pair of TM segments and determined the structure of and examined the importance of the amino acids that appear to be significant in contacts between these segments. The results demonstrate that the TM VI–VII region (TM VI–VII) forms two interacting α-helices, whose structures generally agree with our studies of the single-TM segments.

EXPERIMENTAL PROCEDURES

Materials. Amylose affinity resin was from New England Biolabs (Pickering, ON). Lipofectamine 2000 reagent was from Invitrogen Life Technologies (Carlsbad, CA), and PWO DNA polymerase was from Roche Applied Science (Roche Molecular Biochemicals, Mannheim, Germany). Sulfo-NHS-SS-Biotin was from Pierce Chemical Co. (Rockford, IL).

Expression and Purification of the C-Terminus of NHE1. To produce the TM VI–VII region of human NHE1, we expressed it as a fusion protein with maltose binding protein (MBP) in *E. coli*. We used a modified version of a system described previously.[27] Synthetic DNA encoding amino acids 226–274 of TM VI–VII was purchased from GenScript (GGATCCAAAAAAAAAGATAACTTATTATTCGGTTCTATTATTTCTGCTGTTGATCCAGTTGCTGTTTTAGCTGTTTTCGAAGAAATTCACATTAACGAATTATTACACATTTTAGTTTTCGGTGAATCTTTATTAAACGATGCTGTTACTGTTGTTTTATATAAAAAAAAATGAGAATTC). The *Bam*HI–*Eco*RI sites of the pUC57-TM VI–VII plasmid were used to clone the DNA into vector pMPLB[27] after removal of the inset in the vector with *Bam*HI and *Eco*RI. This created an inducible plasmid expressing maltose binding protein fused to TM VI–VII with a cleavable TEV site separating the maltose binding protein and TM VI–VII (pMBPVI-VII). The DNA sequence was codon optimized for expression in *E. coli*. Polylysine sequences were added at both ends of the peptide region to aid in solubility as described previously.[23] After cleavage with TEV protease, this resulted in a peptide with a GSKKKDNLLFGSIISAVDPVAVLAVFEEIHINELLHILVFGESLLNDAVTVVLYKKK (the N-terminal GS being the result of cloning and from part of the TEV cleavage site) sequence.

Plasmid pMBPVI-VII was transformed into several *E. coli* strains, including XL1 blue, DH5α, BL21(DE-3)pLysS Star, Topp 10, and Topp 11. After trials with different strains and temperatures (not shown), XL1 blue cells were chosen for growth at 37 °C in LB medium and induction at an OD_{600} of ≈1.0 with 0.2 mM IPTG for 16 h. The cells were harvested at 4 °C by centrifugation at 6000*g* for 30 min. Pellets from 1 L cultures were resuspended in 50 mL of amylose buffer [20 mM Tris-HCl, 200 mM NaCl, and 1 mM EDTA (pH 7.4)], divided into two parts, and stored at −80 °C. Preliminary experiments produced unlabeled protein. Later experiments produced ^{15}N-labeled protein for more detailed characterization of the structure. For these experiments, cells were prepared essentially as described previously.[28] *E. coli* cells were grown in a minimal medium made of 87 mM NaH_2PO_4, 34 mM K_2HPO_4, 4 mM $MgSO_4$, 1.8 μM $FeSO_4$, and 55.5 mM glucose (pH 7.3). The medium was supplemented with 1 g of $(^{15}NH_4)_2SO_4$. Minimal medium was inoculated with 40 mL of preculture, and the culture was grown in a 5 L fermenter (BIOSTAT B from B. Braun Biotech International) at 37 °C, 500 rpm, and pH 7.0 until an OD_{600} of 0.8–1.0 was reached. Induction was achieved with 0.2 mM IPTG, and the balance of procedures was as described above for unlabeled protein.

The cell pellet solution was thawed, and cells were lysed using an EmulsiFlex homogenizer at 15000–20000 psi. Homogenization was repeated six times at 4 °C. The lysate suspension was centrifuged at 50000*g* for 30 min at 4 °C, and the supernatant was collected and stored on ice. Aliquots (30 mL) of the supernatant were applied to a column with amylose resin in amylose buffer. The column was washed with 4 column volumes of amylose buffer, and elution was achieved with 2.5 column volumes of amylose buffer containing 40 mM maltose. Samples of the lysate and eluted fractions were examined by sodium dodecyl sulfate–polyacrylamide gel electrophoresis (SDS–PAGE).

MBP–TM VI–VII Cleavage and Peptide Isolation. The eluted fractions were concentrated to 5 mg/mL using an Amicon-15 Ultra 30000 molecular weight cutoff filter at 4300 rpm and 4 °C. Proteolysis of the fusion protein was achieved by incubating the fusion protein with 10 units of TEV protease/mg of peptide at 21 °C overnight. This caused the TM VI–VII peptide to come out of solution, so the sample containing the MBP protein and TM VI–VII peptide was centrifuged at 100000*g* for 45 min at 4 °C and the supernatant containing mostly maltose binding protein discarded. The pellet was made up in 20 mL/100 mg of digested protein in resuspension buffer 1 [50 mM phosphate (Na_2HPO_4/NaH_2PO_4) (pH 8.0) and plus 1 M guanidine-HCl], using a glass homogenizer, and incubated for 30 min at room temperature. This sample was centrifuged at 10000*g* for 20 min at 4 °C. The pellet, which was rich in TM VI–VII peptide, was made up in 5 mL/100 mg of digested protein in resuspension buffer 2 [50 mM phosphate (Na_2HPO_4) (pH 7.2) and 7 M guanidine-HCl]. This sample was centrifuged at 10000*g* for 10 min at 4 °C, and the supernatant was collected. Samples (50 μL) were saved in each step to be analyzed in 16% Tricine–SDS–PAGE gels containing 6 M urea.[29]

The TM VI–VII peptide in 7 M guanidine-HCl was purified using the facilities of the Institute for Biomolecular Design at the University of Alberta. It was applied onto a reverse phase Zorbax 300SB-C8 column (9.4 mm × 250 mm, 5 μm particle size, Agilent Technologies). Buffer A consisted of 0.1% trifluoroacetic acid in water and buffer B 0.1% trifluoroacetic acid in acetonitrile. The column was equilibrated with buffer A at a flow rate of 2.0 mL/min. The peptide was injected, and a linear gradient from 20 to 80% buffer B was run for 135 min. The fractions were collected every minute and analyzed using a narrow bore reversed phase high-performance liquid chromatography (HPLC) system (Supelco Discovery C18 column, 5 μm, 2.1 mm × 125 mm). Buffer A and buffer B were used, and the gradient was from 20 to 98% buffer B over 35 min.

dx.doi.org/10.1021/bi500392y | *Biochemistry* 2014, 53, 3658–3670

Fractions were analyzed by matrix-assisted laser desorption ionization time-of-flight (MALDI-TOF mass spectrometry. TM VI−VII-containing fractions were pooled and lyophilized.

NMR Spectroscopy and Structure Calculation. Samples for NMR spectroscopy contained 0.5−1 mM HPLC-purified TM VI−VII peptide dissolved in perdeuterated dodecylphosphocholine (DPC) micelles in a 1:75 peptide:detergent molar ratio, with 5% D_2O as a lock solvent and 0.25 mM deuterated 4,4-dimethyl-4-silapentane-1-sulfonic acid as an internal chemical shift reference. Samples also contained 1% protease inhibitor (Calbiochem protease inhibitor cocktail set I). The pH was adjusted to 5, and NMR spectra were acquired at 30 °C. Spectra for structure determination were initially acquired with a non-^{15}N-labeled peptide, and additional data were later acquired for a ^{15}N-labeled peptide. One-dimensional (1D) ^{1}H and two-dimensional (2D) ^{1}H−^{1}H DQFCOSY, TOCSY (60 ms mixing time), and NOESY (200 ms mixing time) NMR spectra were acquired on a Varian 800 MHz spectrometer for an unlabeled sample. An additional NOESY spectrum was also acquired at 800 MHz in 100% D_2O with a 400 ms mixing time. 2D ^{15}N HSQC and three-dimensional (3D) ^{15}N NOESY-HSQC (150 ms mixing time) spectra were acquired at 800 MHz on a ^{15}N-labeled sample, and 3D ^{15}N TOCSY-HSQC spectra were acquired on a 600 MHz spectrometer. NMR spectra were acquired using VnmrJ (Agilent Technologies, Santa Clara, CA) and processed using NMRPipe.[30] Spectra were analyzed using NMRViewJ.[31] Sequential assignment followed standard procedures.[32] Peaks were manually assigned in NMRViewJ. Distance restraints for structure calculation were obtained from the 2D NOESY and 3D NOESY-HSQC spectra by calibrating peaks based on intensity in NMRViewJ. Dihedral angle restraints were generated on the basis of Hα secondary chemical shift deviations.[33] Structures were calculated as previously described[34] using simulated annealing in Xplor-NIH.[35] In each round of structure calculation, 50 structures were generated and violating restraints were examined and either lengthened or removed. The cutoff for violations increased in stringency each round. The final round of structure calculation had distance restraint violation cutoffs of 0.1 Å and considered violations that occurred in >10% of structures. The 25 lowest-energy structures were used for analysis. The structures are deposited in the Protein Data Bank (entry 2MDF) and the chemical shifts in the Biomagnetic Resonance Bank (entry 19484).

T_1 and T_2 NMR relaxation measurements were acquired on a 600 MHz NMR spectrometer. 2D ^{15}N HSQC spectra were acquired using the gNhsqc pulse sequence in VnmrJ with an initial 4 s delay and relaxation times of 0.1, 0.3, 0.5, 0.7, 0.9, 1.1, and 1.3 s for T_1 measurements and 0.01, 0.03, 0.05, 0.07, 0.09, 0.11, and 0.13 s for T_2 measurements. Spectra were processed in NMRPipe and assigned in NMRViewJ. T_1 and T_2 values were obtained by fitting peak intensities to an exponential decay curve within NMRViewJ.

Cell Culture and Transfections. To examine the NHE1 activity of mutants, stable cell lines were made using AP-1 cells transformed with control and mutant pYN4+ DNA.[26] AP-1 cells constitute a CHO derivative that lacks its own Na^+/H^+ exchanger protein. Transfection was performed using LIPOFECTAMINE 2000 Reagent (Invitrogen Life Technologies).[36] Stable cell lines for experiments were re-established from frozen stocks at passage numbers between 5 and 9. At least two independently made clones were isolated from different individual transformed cells of each mutant, and results are shown from one typical mutant.

Electrophoresis and Immunoblotting. Cell lysates were made from stable cell lines of NHE1 expressing AP-1 cells as described previously.[36] They were used for Western blot analysis on 10% SDS−PAGE gels as described previously.[37] Identification of the Na^+/H^+ exchanger protein was achieved via the HA tag using an anti-HA monoclonal antibody. The secondary antibody was a peroxidase-conjugated goat anti-mouse antibody, and chemiluminescence was used to visualize the immunoreactive protein. Quantification of expression levels was conducted using ImageJ version 1.35 (National Institutes of Health, Bethesda, MD) as described previously.[36]

Site-Directed Mutagenesis. For mutagenesis of Na^+/H^+ exchanger protein isoform 1, we used expression plasmid pYN4+ that contains a functional HA-tagged, human Na^+/H^+ exchanger.[36] The mutations made and the primers used are listed in Table 1 of the Supporting Information and were made as described previously.[28] Mutations created or deleted a restriction enzyme site used in screening for mutants. DNA sequencing was used to confirm the mutation and fidelity of DNA amplification.

Cell Surface Expression. Cell surface expression was assessed essentially as described previously.[28] Briefly, the surface proteins of intact cells were labeled with sulfo-NHS-SS-biotin (Pierce), and immobilized streptavidin resin was used to bind the solubilized plasma membrane Na^+/H^+ exchanger. Equal amounts of total and unbound proteins were separated by SDS−PAGE and analyzed using Western blotting and densitometry measuring immunoreactive (HA-tagged) Na^+/H^+ exchanger protein. As it was not possible to efficiently and reproducibly elute proteins bound to immobilized streptavidin resin, the relative amount of NHE1 on the cell surface was calculated by comparing both the 110 and 95 kDa HA-immunoreactive species in Western blots of the total and unbound fractions.

Measurement of NHE Activity. NHE1 activity was determined using a PTI Deltascan spectrofluorometer essentially as described previously.[28,38] Briefly, experiments were performed at 37 °C, and stable cells lines of NHE1 mutants were grown on coverslips (Thomas Red Label Micro Cover Glasses) in 35 mm dishes until the cells were approximately 80−90% confluent. BCECF-AM [2′,7′-bis(2-carboxyethyl)-5(6)-carboxyfluorescein acetoxymethyl ester] (Molecular Probes Inc., Eugene, OR) was used to measure the intracellular pH in normal buffer [135 mM NaCl, 5 mM KCl, 1.8 mM $CaCl_2$, 1 mM $MgSO_4$, 5.5 mM glucose, and 10 mM HEPES (pH 7.3)]. The cells were treated with 50 mM ammonium chloride for 3 min, after which the solution was changed to isotonic sodium free buffer for 30 s to induce acidification. The cells were then returned to normal sodium-containing buffer, allowing the recovery of pH via the activity of NHE1. The first 20 s of recovery was used to calculate the NHE1 activity. Each measurement of NHE1 activity was followed by a three-point pH_i calibration at pH 6, 7, and 8 with 10 μM nigericin in calibration buffer as described previously.[28]

RESULTS

Production and Purification of TM VI−VII. Figure 1 illustrates a simple model of the NHE1 isoform of the Na^+/H^+ exchanger with an enlargement of the TM VI−VII region. While there is currently some controversy about the topology of some parts of the protein with two different models being

dx.doi.org/10.1021/bi500392y | Biochemistry 2014, 53, 3658−3670

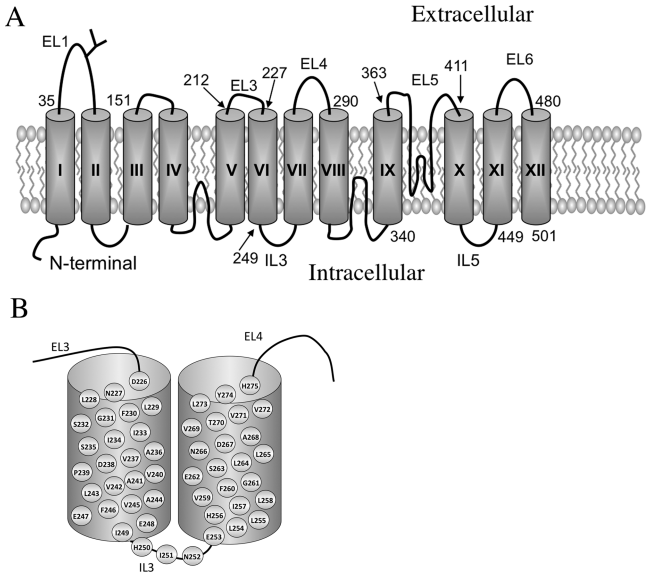

Figure 1. Schematic diagram of the Na^+/H^+ exchanger. (A) Illustration of the entire Na^+/H^+ exchanger protein, isoform 1, based on Cys accessibility studies.[17] (B) Enlargement of the TM VI–VII region showing the amino acid sequence.

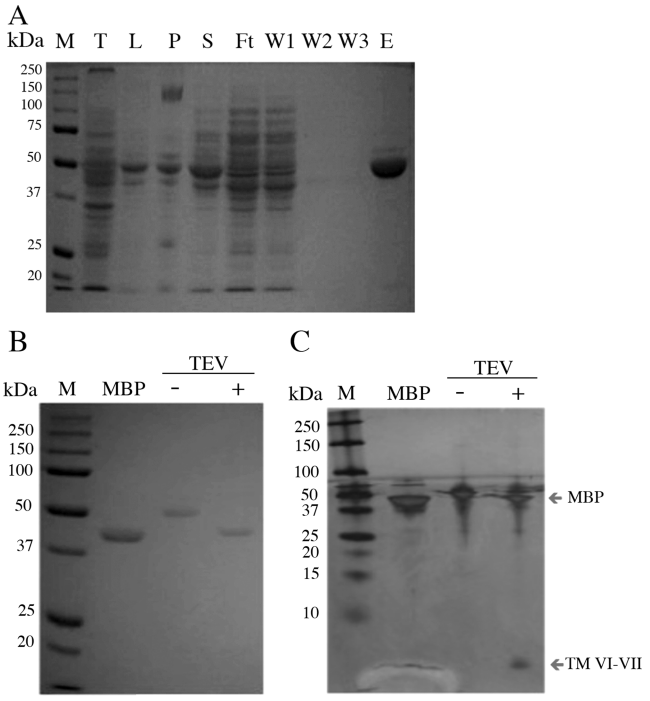

Figure 2. Purification of TM VI–VII. (A) Coomassie blue-stained protein gel showing steps in maltose binding protein–TM VI–VII purification with amylose resin. Elution was conducted with 40 mM maltose. Lanes: M, molecular weight markers; T, XL1 blue cells at time zero (prior to induction); L, lysate after induction for 20 h at 37 °C with 0.2 mM IPTG; P, 50000*g* pellet of lysed cells; S, supernatant of lysed cells; Ft, flow through of the column; W1–W3, column washes; E, protein eluted with maltose. (B and C) Samples of purified maltose binding protein (MBP, not linked to any other protein) and MBP–TM VI–VII protein without (−) or with (+) TEV treatment. (B) Standard 11% SDS–PAGE, stained with Coomassie Blue. (C) Tricine–SDS–PAGE (16%), stained with silver.

prevalent,[17−19,39] there is no discordance regarding the region containing amino acids 226–275. Amino acids 226–247 are believed to constitute a TM segment, leading to a short intracellular loop (IL3, amino acids 248–252), which connects to another TM segment comprised approximately of amino acids 253–275. Because the connection between amino acids 226–247 and 253–275 is quite short, this suggests that these TM segments must be in the proximity of one another.

To examine the structure of TM VI–VII, we overexpressed the two-transmembrane segments in *E. coli* and purified the resultant protein. Previously, we expressed single-TM segments in *E. coli* and examined the structure of single-transmembrane segments.[23,26,28,40] Because of the inherent difficulties in expression of membrane proteins in *E. coli*, we used a strategy in which the TM segments are expressed as a fusion with maltose binding protein that enhances the solubility and expression in *E. coli* and aids in purification.[27] After construction of an appropriate fusion protein (see Experimental Procedures), several *E. coli* strains were checked for their efficacy in expression of the maltose binding protein–TM VI–VII protein [XL1 blue, DH5-α, BL21(DE-3), BL21(DE-3)pLysS Star, Topp 10, and Topp 11] at 20 and 37 °C. The best result was obtained using XL1 blue cells, at 37 °C with 0.2 mM IPTG used for induction. This yielded approximately 400 mg of fusion protein per liter of culture (data not shown). The expressed protein was purified and cleaved free of the maltose binding protein carrier. Figure 2 shows the results. Purification of the MBP–TM VI–VII protein via affinity chromatography yielded highly purified protein (Figure 2A). Treatment with TEV protease resulted in efficient cleavage and release of a TM VI–VII peptide, which was visible when electrophoresis was conducted in higher-percentage acrylamide gels (Figure 2B,C).

After cleavage, the TM VI-VII protein was relatively insoluble and easily pelleted. It was selectively solubilized and purified by reverse phase HPLC as described in Experimental Procedures. Fractions were analyzed by MALDI-TOF mass spectrometry, and the molecular weight of the resulting peptide corresponded to the predicted molecular mass. Approximately 10 mg of pure TM VI–VII peptide was obtained per liter of *E. coli* culture. The same procedure conducted in ^{15}N-labeled minimal medium yielded approximately 5 mg/L of culture, and the molecular mass determined by mass spectroscopy was shifted exactly in accordance with the mass change caused by ^{15}N isotopic labeling.

Structural Analysis of TM VI–VII. Initial characterization of the purified TM VI–VII peptide in DPC micelles utilized the 1D ^1H NMR spectra of non-isotopically labeled peptide samples. NMR spectra with well-resolved and reasonably narrow amide peaks were obtained under the conditions used in our previous NMR studies of single-TM segments of NHE1.[23,26] Increasing the temperature to 40 °C did not appear to improve the spectral quality, and increasing the pH to 6 decreased the quality slightly; therefore, spectra were obtained at 30 °C and pH 5 for structure determination. ^{15}N isotopically labeled peptide samples showed 2D $^1H-^{15}N$ HSQC NMR spectra with good resolution and dispersion of peaks and allowed for 3D NMR experiments for assignment and structure calculation as well as ^{15}N relaxation measurements. The amide proton region of the 1D ^1H NMR spectrum and the assigned 2D $^1H-^{15}N$ HSQC NMR spectrum are shown in Figure 3.

The peptide was assigned using standard methods[32] using homonuclear 2D $^1H-^1H$ TOCSY, NOESY, and DQFCOSY NMR spectra. The chemical shifts of some residues were similar those of the previously assigned individual TM VI[23] and

dx.doi.org/10.1021/bi500392y | *Biochemistry* 2014, 53, 3658–3670

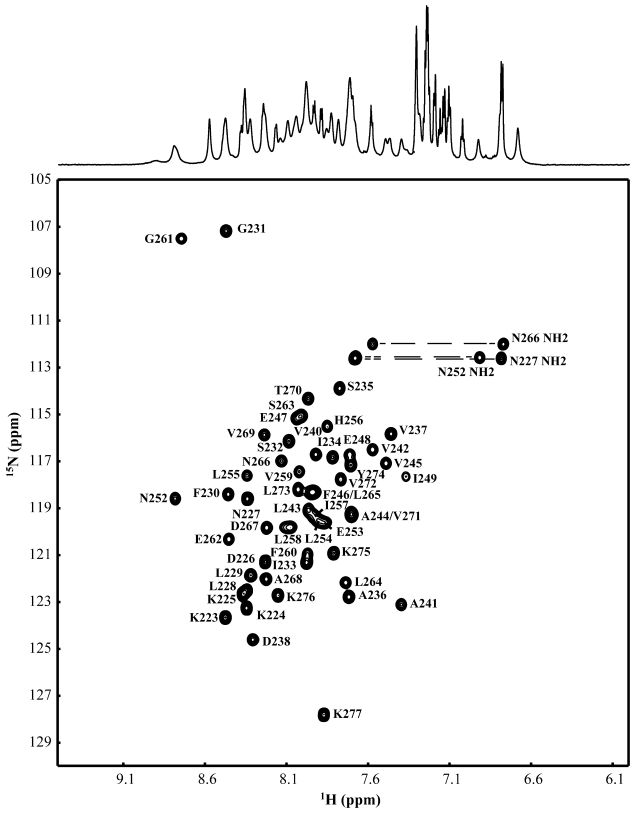

Figure 3. NMR spectra of TM VI–VII in DPC micelles: (top) amide/aromatic region of the 1D ^{1}H NMR spectrum of the unlabeled TM VI–VII peptide, showing amide, amine, and aromatic peaks, and (bottom) corresponding region from a 2D ^{1}H–^{15}N HSQC spectrum of ^{15}N-labeled TM VI–VII showing only amide peaks, with peak assignments shown.

TM VII[26] peptides, which aided the assignment process. The amide cross-peaks in the 2D ^{1}H–^{15}N HSQC NMR spectrum were assigned using 3D ^{1}H–^{15}N TOCSY and NOESY HSQC NMR spectra, which also provided additional structural restraints.

The distance restraints obtaining using the 2D and 3D NOESY spectra with mixing times of 150–200 ms were used to generate structural models of the peptide. A further 2D homonuclear NOESY spectrum with a longer mixing time of 400 ms in D_2O was used to help look for methyl and aromatic side chain contacts. The distance restraints observed are summarized in Figure 4. The $d(i,i+3)$ and $d(i,i+4)$ NOESY contacts and the negative deviations of Hα chemical shifts from random coil chemical shifts[33] suggest that the α-helical regions are in agreement with the previously published TM structures. NOE distance restraints were calibrated on the basis of peak intensity rather than volume because of peak overlap, and an iterative procedure was used to relax the restraints for the same reason. Dihedral angle restraints were based on chemical shift index predictions and preliminary structure calculations that did not use dihedral restraints. Helical regions were restrained to a φ of $-60 \pm 30°$ and a ψ of $-40 \pm 40°$. Statistics from the final 25 of 50 structures are listed in Table 1.

The secondary structure of the final 25 structures agrees with the NMR distance and dihedral restraints. The dihedral angle order parameters (bottom panel of Figure 4) show that TM VI contains two structurally conserved regions corresponding to two short α-helices spanning residues 229–236 in the N-terminus (TM VIn) and 239–247 in the C-terminus (TM VIc). Among the 25 ensemble members, the two short helices do not have a fixed orientation with respect to each other but adopt angles of around 0–90°. TM VI leads into a nonhelical, flexible region (residues 248–254) that forms an interhelical loop. TM VII contains one long helical region between residues 255 and 274. While this helix can be superimposed along its entire length, superimposition over a shorter portion of TM VII reveals some slight differences in the curvature of the TM segment among the ensemble members.

The final 25 structures of TM VI–VII show that the two TM segments are similar to the previously published structures of the corresponding single-TM segments (Figure 5). The overall structure and helix orientations of TM VI are the same between the single-TM peptide reported previously (Figure 5B)[23] and the TM VI–VII peptide in this study (Figure 5A). However, in comparison to the previously published individual TM structures, TM VIc is shorter in TM VI–VII, while in the single-TM peptide, it extends further to include H250 and two of the three lysine tags (numbered 251–253). These lysine tags are not present in the TM VI–VII peptide, which contains only the native loop residues.

There is a larger difference between the structures of TM VII in the single-TM study reported previously (Figure 5D)[26] and TM VII in the TM VI-VII peptide reported here (Figure 5C). The major difference between the TM VII structures is that in the single-TM structure of TM VII, a kink is present at residues 260–263 in the middle of the TM that allowed the two halves of TM VII to adopt either a straight or hairpin conformation. In comparison, TM VII of the TM VI–VII structure forms a straight helix and does not appear to be kinked. The boundaries of TM VII are similar, consisting of residues 254–274 in TM VI–VII compared to residues 255–272 in TM VII. The slight difference at the C-terminal end of TM VII could be due to one additional C-terminal lysine residue present in the TM VI–VII peptide that is not present in the single-TM peptide.

T_1 and T_2 relaxation measurements provide a measure of the motional properties of the peptide and are consistent with the secondary structure. The T_1/T_2 ratio is proportional to the local rate of motion in the molecule, with lower ratios corresponding to more mobile regions and higher ratios to less mobile regions (Figure 6). The low T_1/T_2 ratio at the termini suggests that the termini (residues 221–228 and 274–277) are quite mobile. Values increase up to plateau regions, which correspond to the location of the α-helices in the NMR structures. TM VIn has a T_1/T_2 ratio lower than that of TM VIc, suggesting the N-terminal helix is more mobile than the C-terminal helix. Interestingly, TM VIc has a T_1/T_2 ratio similar to that of TM VII, suggesting they have similar mobilities, even though TM VIc is approximately half the size of TM VII. This could suggest that there is interaction between TM VI and TM VII. The connecting loop between TM VI and TM VII may be undergoing slow conformational exchange on microsecond to millisecond time scales, which could explain the decrease in T_2 and the increase in the T_1/T_2 ratio at residues 248 and 249 as well as the disappearance of residues 250 and 251 in the 2D HSQC spectrum. This is also reflected in the structure, where this region has backbone dihedral order parameters lower than those of the surrounding helices (Figure 4). This suggests that the loop does not have a fixed structure; however, interaction between TM VI and TM VII could be partially restricting the conformation of the loop. Reddy et al.[41] published relaxation data at three spectrometer frequencies for a TM VII peptide

dx.doi.org/10.1021/bi500392y | *Biochemistry* 2014, 53, 3658–3670

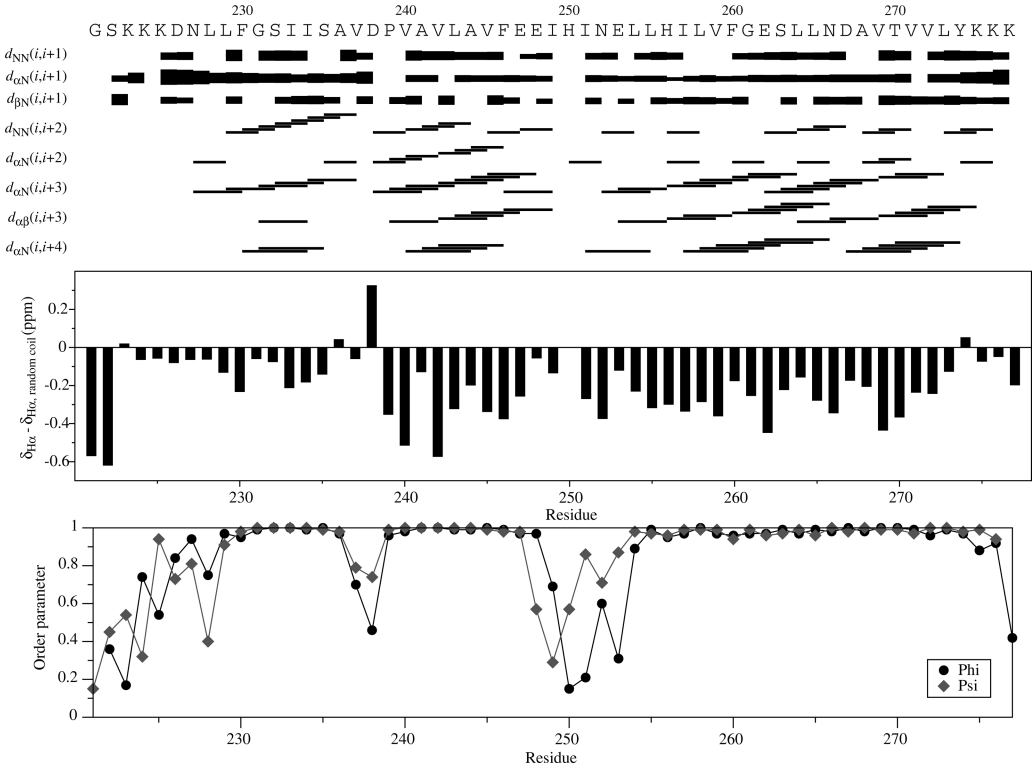

Figure 4. Summary of NMR structural data for TM VI–VII in DPC micelles. The top panel is a summary of short- and medium-range residue distances obtained from the 2D and 3D NOESY NMR spectra. Lines and bars represent observed distances between residues. Continuous $d(i,i+3)$ and $d(i,i+4)$ contacts are indicative of helical structure (adopted from CYANA[59] output). The center panel shows the chemical shift index prediction of secondary structure.[33] Contiguous regions of negative deviation of the peptide Hα chemical shifts from random coil chemical shifts suggest helical structure. The bottom panel shows dihedral angle order parameters for the final TM VI–VII structural ensemble. Values of 1 represent regions with identical dihedral angles across the structures, while values of 0 represent a random distribution of angles.

Table 1. Structure Calculation Statistics for TM VI–VII in DPC Micelles for the Final Top 25 of 50 Lowest-Energy Structures

NOE restraints	
intraresidue	452
sequential	392
medium-range ($\|i - j\| \leq 4$)	389
long-range ($\|i - j\| > 4$)	31
ambiguous	484
dihedral restraints	
ϕ	35
ψ	35
restraint violations	
NOE (>0.5 Å)	5
dihedral (>5.0°)	2
Ramachandran statistics[a] (%)	
favored regions	58.2
additionally allowed regions	30.5
generously allowed regions	8.6
disallowed regions	2.7

[a]Determined using PROCHECK.[58]

that was labeled with ^{15}N at six residues. A comparison of the data obtained by Reddy et al. and our data is shown in Figure 1S of the Supporting Information. Values for T_2 at 600 MHz are overall slightly higher in the individual TM VII, likely reflecting the smaller size of the single-TM peptide compared to the size of TM VI–VII. T_1 values appear to be similar and perhaps slightly lower for TM VII in TM VI–VII at the C-terminus. T_1/T_2 ratios are larger for TM VII in TM VI–VII on the N-terminus but similar at the C-terminus. Overall, the comparison is consistent with the higher molecular weight of TM VI–VII and lower mobility at the N-terminus of TM VII in the two-TM peptide because of the presence of TM VI.

The calculated structures show a weak interaction between TM VI and TM VII. On the basis of PROMOTIF[42] structural analysis, TM VIn does not interact at all with TM VII, which is consistent with the relaxation results and observed NOE distances. Ten of the 25 final structures show an interaction between TM VIc and TM VII according to PROMOTIF. A representative structure is shown in Figure 7A with the identified long-range restraints shown. Long-range restraints are mainly between residues close to, or within, the interhelical loop. Many contacts originate from F246 and H256, near the ends of the α-helical parts of the TMs, to other residues in the vicinity. NOE contacts between the lower half of TM VIc and TM VII could not be observed, suggesting that in this region TM VIc interacts very weakly or not at all with TM VII. As a result of this, TM VIc does not always lie along TM VII in the structural ensemble but sometimes is oriented perpendicular to TM VII. This conformational flexibility prevents the definition of a precise interface between TM VI and VII. An ensemble of structures showing the potential structures with TM–TM interactions is shown in Figure 7B.

Functional Analysis of TM VI–VII. The region of TM VI, termed TM VIc (amino acids 239–247), was helical in character and showed some interactions with TM VII along at least part of its length in the NMR structure. To gain further insight into the interactions between TM VI and TM VII and

dx.doi.org/10.1021/bi500392y | Biochemistry 2014, 53, 3658–3670

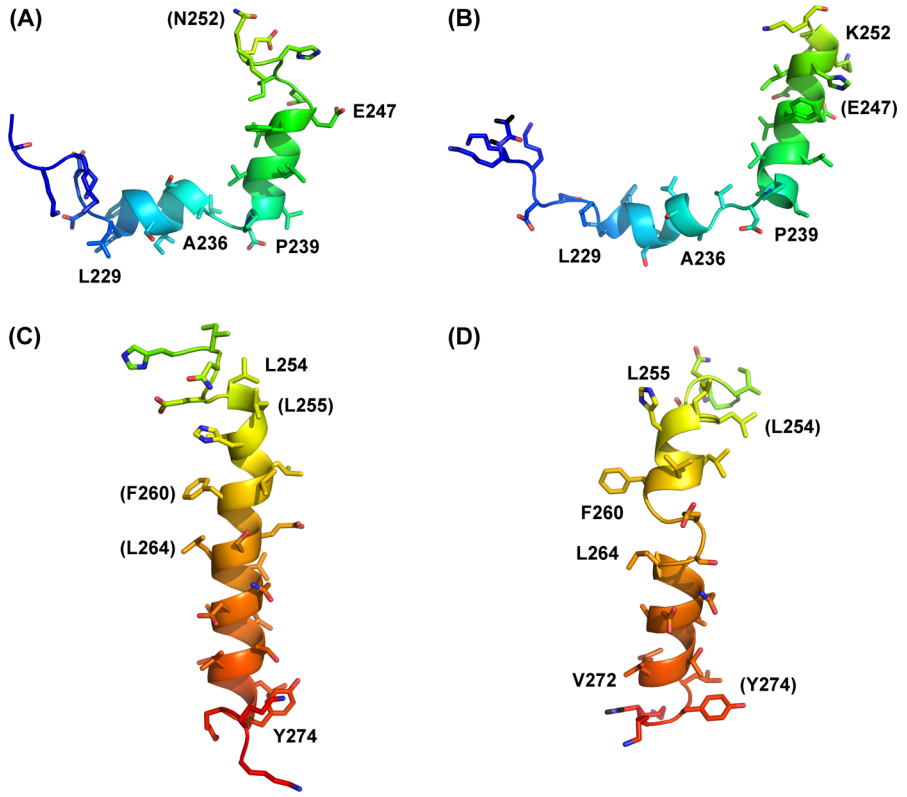

Figure 5. Comparisons of the TM segments of TM VI–VII with previously published structures. Comparisons of TM VI (residues 221–250) (A) and TM VII (residues 250–277) (C) from the structure of TM VI–VII in this study with the individual TM VI (residues 223–253) (B) and TM VII (residues 250–276) (D) structures described previously.[23,26] The residues at the ends of α-helical segments are labeled. Residues in parentheses are the helix termini of the opposing one- or two-TM structure.

to study the role of particular amino acids V240–E247, we used Trp scanning mutagenesis. Initial experiments examined effects of mutations (V240W, A241W, V242W, L243W, A244W, V245W, F246W, E247W, V237L/L264V, V242F/F260V, and F246I/I257F) on expression (Figure 8A) and targeting (Figure 8B) of mutant NHE1 proteins. Most mutation-containing NHE1 proteins were expressed very well, with the exception that the protein with a V242W mutation was poorly expressed relative to the other proteins. Surface targeting of the various mutant proteins varied somewhat, though most were targeted reasonably well to the cell surface. The F246W mutant was slightly reduced in surface targeting somewhat compared to the wild type and other mutants.

Characterization of the activity of the wild-type and mutant proteins is shown in Figure 8C–E. Figure 8C is an example of activity measurements of mutants of NHE1, and Figure 8D shows a summary of the basal activity of some of the mutants examined. Wild-type NHE1 protein expressed in AP-1 cells showed a rapid and robust recovery from transient acidosis induced by an ammonium chloride pulse. In contrast, mutants V240W to V245W all showed no significant activity greater than background. An example of the inactive V240W mutant is shown in Figure 8C. Mutants F246W and E247W had some remaining activity. Much of the apparent decrease in their activity was due to a reduction of the protein's level of expression and targeting to the cell surface (Figure 8D).

To ensure that activity we measured was due to the Na^+/H^+ exchanger, we examined the effect of the NHE1 specific inhibitor EMD87580 on the activity of the wild-type and mutant Na^+/H^+ exchanger proteins. Figure 8E illustrates the results. Experiments were conducted using a two-pulse assay,[26] with two ammonium chloride loads, with 10 μM EMD87580 added in the second recovery. Uninhibited NHE1 had the same activity in the second pulse as in the first.[26] The addition of 10 μM EMD87580 essentially eliminated NHE1 activity. Another control was the removal of extracellular sodium from the medium, which eliminated the recovery from acidosis (Figure 8E). A different control (Figure 8E) showed that under the conditions used in our assay, there was no recovery from the acid load in AP-1 cells that are devoid of NHE1 protein. The effects of 10 μM EMD87580 were examined on some of the mutant proteins. EMD8750 caused no effects on inactive mutants from V240 to V245. Effects on mutants V240W and A244W are also shown. The activity of the F246W and E247W mutants was eliminated by the addition of 10 μM EMD87580 in the recovery phase, confirming that it was due to the NHE1 protein.

An examination of the NMR structures of TM VI–VII revealed that several pairs of residues on TM VI and TM VII were opposed to each other, possibly an indication of an association in the intact full length protein. This included the V237–L264, V242–F260, and F246–I257 pairs. We reasoned that the interaction of the side chains of these putative pairs of amino acids might be mimicked and confirmed this by reciprocal mutations, which switched the pairs of amino acids (V237L/L264V, V242F/F260V, and F246I/I257F). These mutations were made, and the activity of the intact full length protein was examined as described above (Figure 9). Mutant proteins V237L/L264V and F246I/I257F showed no NHE1 activity. In contrast, the V242F/F260V mutant exhibited ~30%

dx.doi.org/10.1021/bi500392y | *Biochemistry* 2014, 53, 3658–3670

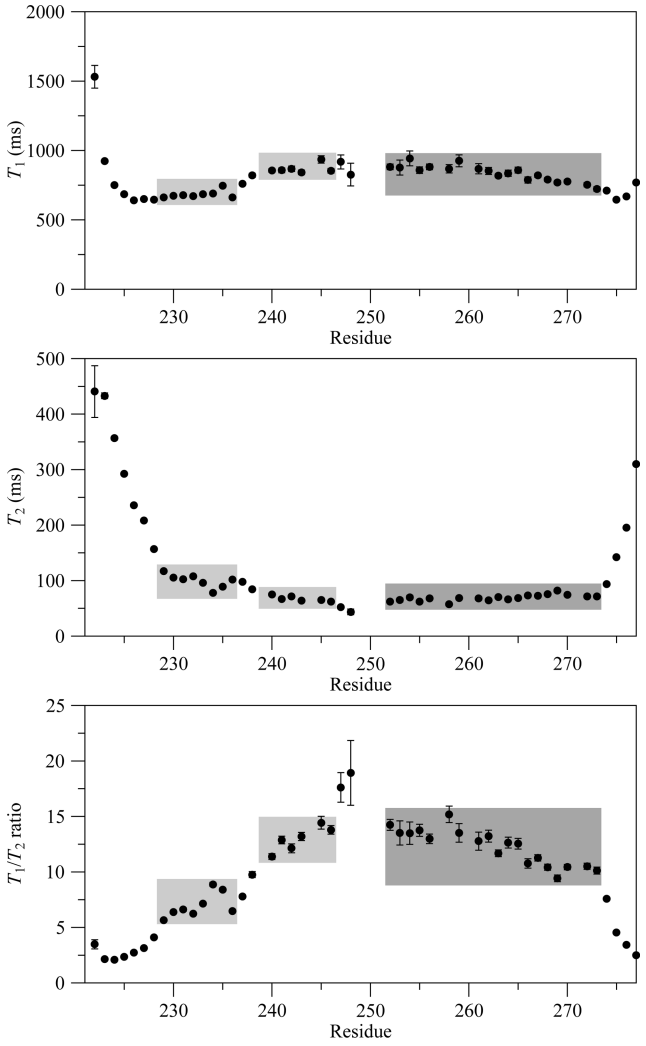

Figure 6. ^{15}N NMR T_1 and T_2 relaxation times and T_1/T_2 ratios for TM VI–VII in DPC micelles. Plateau regions represent the helical regions as also determined by NOE and chemical shift NMR data. Helical regions of TM VI are colored light gray and those of TM VII dark gray.

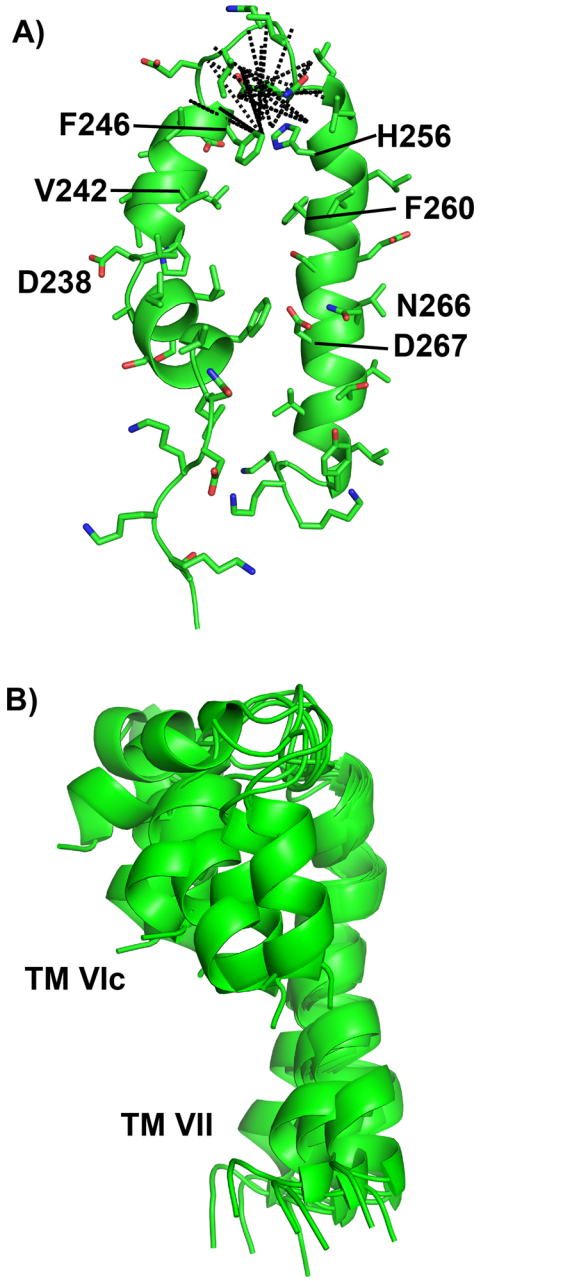

Figure 7. Structure of TM VI–VII in DPC micelles. (A) Representative structure of TM VI–VII showing TM–TM interactions, with the observed long-range NOE restraints used in the structure calculation shown as dotted lines. Some amino acids that are functionally important or were found to interact in this study are labeled. (B) Superimposition of the 10 members of the structural ensemble of TM VI–VII that contain TM–TM interactions as defined by PROMOTIF. The structures are superimposed over the backbone Cα atoms of residues 254–264 of TM VI–VII. Residues 220–237 of TM VI are not shown for the sake of clarity.

of the activity of the wild-type protein, which was inhibited by EMD87580. Mutant NHE1 proteins with an individual V242F or F260V mutation showed no activity.

DISCUSSION

Membrane proteins are of great interest in modern biology. They are key regulators of cellular milieu, participate in signal transduction, and are involved in a variety of human diseases, including cystic fibrosis, muscular dystrophy, and others. Additionally, they are often the targets of drug treatments, particularly in the case of plasma membrane proteins that tend to be more accessible to treatment because the compounds need not cross a lipid bilayer to be effective. While of great interest, only a small number of structures of membrane proteins have been elucidated because of the inherent difficulty in expressing and purifying the proteins. We previously used expression systems in *E. coli* to express fragments of the mammalian NHE1 protein. We expressed and examined the structure of putative transmembrane segments TM IV, TM VI, TM VII, TM IX, and TM XI.[23,24,28,43,44] Studies comparing the structure of isolated TM segments with that of the intact full length protein suggested that much of the final higher-order structure of the segments is determined by the primary sequence.[20−22,45,46]

Though we gained several important insights into NHE1 function by studying single-TM segments, it is not possible to gain a complete picture of eukaryotic protein function using single-TM segments. Production of the entire membrane domain of multiple-pass eukaryotic membrane proteins remains

dx.doi.org/10.1021/bi500392y | *Biochemistry* 2014, 53, 3658−3670

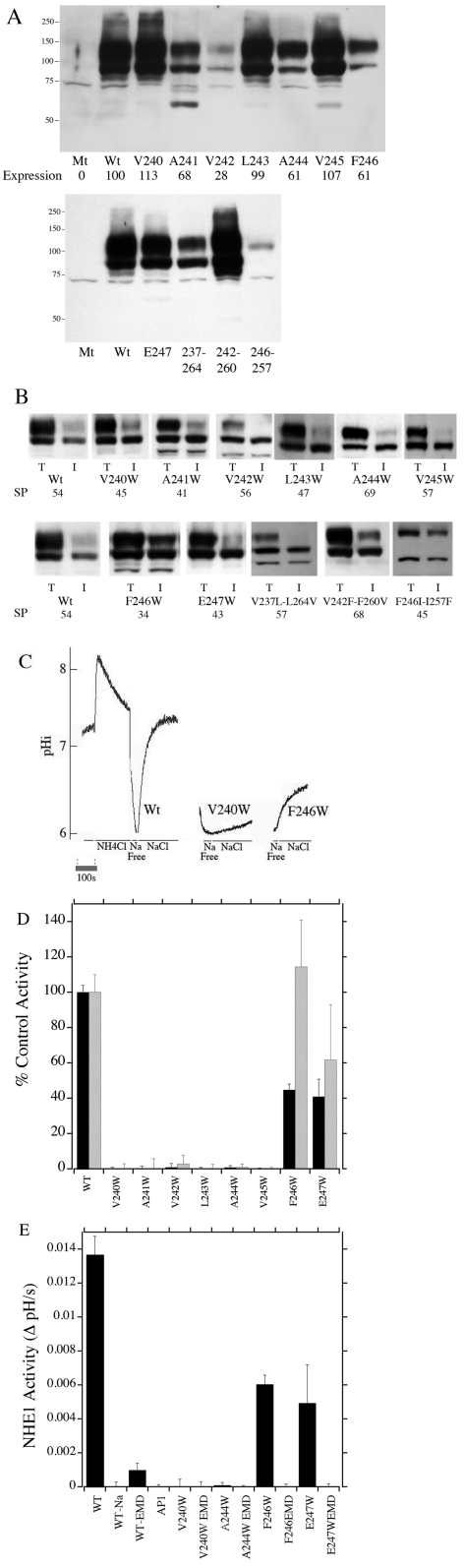

Figure 8. Characterization of activity and expression of Trp scanning mutants of TM VI–VII. (A) Western blot of cell extracts of stable transfectants expressing Na^+/H^+ exchanger mutants or control proteins. Mutants are V240W, A241W, V242W, L243W, A244W, V245W, F246W, E247W, V237L/L264V, V242F/F260V, and F246I/I257F. Mt denotes mock transfected AP1 cells and Wt wild-type NHE1. Numbers underneath mutants indicate expression levels as a percentage of the control (n = 3). Densitometric scans were of both the 110 and 95 kDa bands relative to wild-type NHE. (B) Surface

Figure 8. continued

localization of NHE1-transfected cells expressing control and mutants. Equal amounts of the total cell lysate (left lane, T, total) and unbound intracellular lysate (right lane, I, intracellular) were examined by Western blotting with the anti-HA antibody to identify NHE1 protein. SP denotes surface processing, with mean values (n = 3) being a percentage of NHE1 targeted to the cell surface. Wt denotes wild-type NHE1 protein. Film exposure times were increased for mutants expressing lower levels of protein. (C) Example of the measurement of activity of NHE1 and Trp scanning mutants. NHE1 protein activity was assayed after ammonium chloride-induced acid load in stably transfected AP-1 cells. Traces are shown for the entire ammonium chloride treatment and recovery of wild-type NHE1. For the sake of clarity, only the recovery from acidosis is shown for V240W and F246W. (D) Summary of the rate of recovery from an acute acid load of AP-1 cells transfected with wild-type NHE1 and the indicted Na^+/H^+ exchanger mutants. The mean activity of wild-type NHE1 stably transfected with NHE1 was 0.012 ΔpH/s. This value was set to 100%, and other activities are a percent of those of wild-type NHE. Values are means ± the standard error of 8–12 determinations. Results are shown for mean activity of both uncorrected (black) and normalized expression levels (striped) and surface processing (measured as in panels A and B). (E) Measurement of NHE1 protein activity in the presence or absence of 10 μM EMD87580. For these experiments, cells were given two pulses of ammonium chloride followed by recovery in sodium-containing medium, as described previously.[26] The second recovery was in the presence of 10 μM EMD87580, a specific NHE1 inhibitor,[26] and the rate of recovery in the presence of EMD87580 was compared to that without the inhibitor. We demonstrated previously[26] that when cells are treated with repetitive ammonium chloride pulses followed by recoveries, the second recovery is equivalent to the first (in the absence of additional reagents).

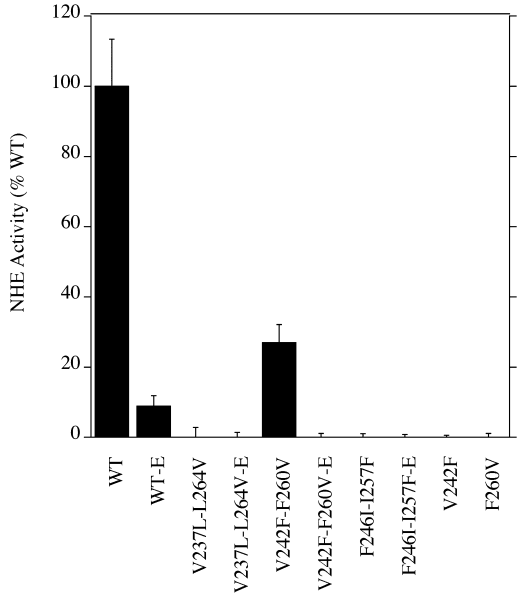

Figure 9. Characterization of the activity of wild-type (WT) and mutant NHE1 proteins. The activity of NHE1 proteins expressed in AP-1 cells is expressed relative to that of the wild-type protein. Mutants are double mutants V237L/L264V, V242F/F260V, and F246I/I257F and single mutants V242F and F260V. The suffix E indicates the addition of 10 μM EMD87580 in the recovery phase. The background activity (recovery or drift in pH_i in the absence of sodium) was subtracted from all proteins.

dx.doi.org/10.1021/bi500392y | *Biochemistry* 2014, 53, 3658–3670

problematic. Modeling can provide insights into their structure, but it ultimately needs to be verified. Here, we expanded our previous procedures in which we examined single-TM segments. Two TM segments of the NHE1 protein, TM VI–VII, were produced and purified, and their structural and functional characteristics were studied. We were able to produce this two-TM segment using many of the same techniques described previously,[28] though larger regions are as yet refractory to expression (not shown).

Landau et al.[18] suggest that the TM VI–VII region examined in this paper is equivalent to TM 4–5 in NhaA, based on homology modeling and evolutionary conservation analyses. TM 4 of NhaA contains two short helices separated by an extended region and contains a functionally important, conserved aspartate (D133) at the start of the C-terminal helix.[47] TM 5 of NhaA is a straight helix containing two conserved and functionally important aspartate residues (D163 and D164) involved in ion binding and transport.[48] The two TMs are connected by an approximately five-residue loop. In a three-dimensional model of NHE1 published by Landau et al.[18] based on the NhaA structure, TM VI–VII of NHE1 shows the same features as TM 4–5 of NhaA. The model has TM VI positioned such that the extended region is placed near the side chains of N266 and D267 in TM VII, where these conserved charged and polar residues might play a role in the ion binding and transport mechanism similar to the role of D163 and D164 in NhaA. They further orient TM VI and TM VII such that on the cytoplasmic halves of TM VI and TM VII, residues P239, V242, L243, and F246 on TM VI and L255, H256, V259, V260, and S263 on TM VII as well as N266 and D267 form a face over which the TM segments interact. However, the extracellular ends of the segments do not interact as strongly in the model or in NhaA.

Our NMR studies of TM VI–VII show that the individual segments have a structure similar to that of TM 4–5 in NhaA, with TM VI showing a discontinuous structure and TM VII a straight helix. Interactions between the N-terminal and extended region of TM VI to TM VII could not be observed; therefore, TM VI does not lie completely along TM VII in the NMR structure as it does in the Landau model, and the extended region comes close to N266 and D267 of TM VII only in a few structures. Interactions are observed only in and around the interhelical loop, with interactions between TM VIc and TM VIIn including the two aromatic residues, as described above, loosely resembling the structure predicted in the Landau model.[18] The structure of TM VI–VII is also supported by recent structures of NhaP1,[49] ASBT,[50] and NapA,[51] all of which share the same fold with NhaA and the Landau model, including the critical TM 4–5 of NhaA.

While it was not possible to directly observe interactions more distal from the interhelical loop in the NMR structure, experiments using site specific mutagenesis support the suggestion that amino acids near this region may be interacting with TM VII. We used tryptophan scanning mutagenesis to disrupt interactions of the transmembrane segments. This procedure has been used previously[52−55] with the large size of the tryptophan residue used to disrupt TM segment association. Insertion of a Trp residue into TM VI from amino acid V240 to V245 abolished NHE1 activity. We demonstrated that the loss of activity was not due to a lack of expression of the protein or to mistargeting of the protein. The changes in surface processing and targeting of NHE1 could not account for the abolition of activity. This suggested that at least some of the amino acids of this region might interact with another TM segment, likely TM VII. These results are in agreement with modeling that suggests TM VI and TM VII interact over this region.[18] We previously used cysteine scanning mutagenesis and replaced amino acids of this region with Cys residues.[23] Amino acids 240–246 retained activity when they were changed to Cys, though amino acid E247 was inactive when it was changed to Cys. Because a Cys residue was tolerated at amino acids 240–246 while the larger Trp residue was not, it is likely that the bulky size of the Trp is critical in disrupting NHE1 activity. It was notable that all of the NHE1 mutants to Trp from V240 to V245 were inactive. Others[54,55] have shown Trp scanning mutagenesis can have a periodic profile of effects on expression, structure, and activity. This is attributed to an effect on either a membrane protein pore or a helical face of a TM segment. Our results suggest that in NHE1 this entire region of TM VI is critical.

Interestingly, in our earlier study,[23] in which L243 was changed to a Cys, it reacted with [2-(trimethylammonium)-ethyl]methanethiosulfonate, and this inhibited NHE1 activity. A244C and V245C mutant proteins were also less reactive. L243 is a candidate for a pore-lining residue. It may be that L243 is a pore-lining amino acid while other amino acids from position 240 to 245 are more important in TM associations. Insertion of a Trp residue at position 243 could be enough to disrupt the NHE1 pore and inhibit activity.

It is also interesting that the E247C[23] mutant was inactive while the E247W mutant retained activity. These results suggest that in this region, a bulky side chain is not as critical as a change to a Cys residue. Why a change to a Cys residue results in inhibition is not clear at this time.

Another test of the interaction between TM VI and TM VII was to switch pairs of amino acids of the two TM segments. We were able to switch amino acids V242 and F260 of TM VI and TM VII, respectively, to F242 and V260, respectively, and this protein was functional, though at an activity level reduced compared to that of the wild type. Single mutants of these amino acids were not functional, suggesting that an interaction between amino acids at this location may be important.

The interaction of F242 and V260 suggested by mutagenesis supports the NMR structural studies of the TM VI–VII peptide. The structure of this peptide in detergent micelles contained interhelical interactions originating from F246 and H256. These residues would be on the same face of their respective TM segments as F242 and V260 because of the α-helical structure of the segments (Figure 7), and it is likely that these residues could form interactions, as well. The lack of observable interaction between F242 and V260 in the NMR structure, while interactions closer to the interhelical loop were observed, suggests that the peptide is quite flexible in comparison to this region in the full length protein.

Swapping other such pairs of amino acids did not yield an active NHE1 protein. The reason for this is not yet clear. It may be that the altered side chains are not precisely aligned or that an interaction there is not critical and the precise amino acids at these locations have another function.

A comparison of the NMR structure of TM VI–VII and TM 4–5 of NhaA is shown in Figure 10. The weaker interaction of TM VI and TM VII compared to those predicted in the Landau model likely suggests that additional interactions in the full length protein may be important in maintaining the structure of TM VI–VII. This may be by anchoring the free ends of the peptide and providing additional packing constraints to

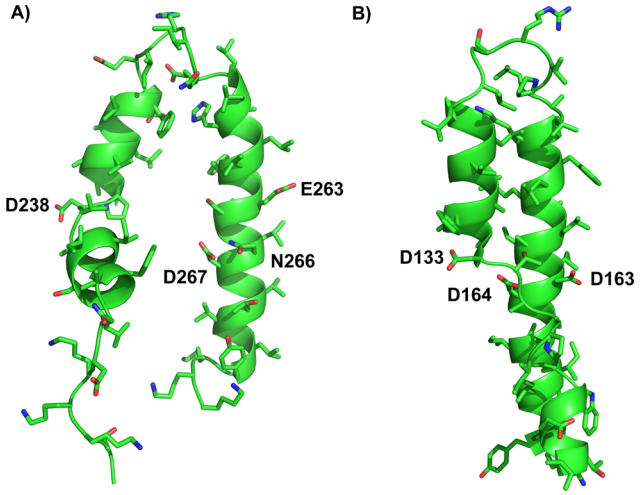

Figure 10. Comparison of a representative NMR structure of TM VI–VII with TM 4–5 of NhaA. (A) Representative NMR structure of the TM VI–VII peptide in DPC micelles determined in this study. (B) TM 4–5 (residues 121–175) of the crystal structure of NhaA.[56] Residues thought to be involved in ion binding and transport are labeled.

encourage the proper interaction of the TM segments. This suggestion is supported by our results with Trp scanning mutagenesis, which sees additional interactions on the same helical face as the residues that can be seen to interact in the NMR structure. Nevertheless, the partial interaction of the two TMs in the NMR structure suggests that the weak interactions in TM VI–VII and the structure of the connecting loop play a role in defining the structure and folding of this region. The crystal structure of NhaA, off which the Landau model is based, is an "acid-locked" inactive state.[56] Conformational changes occur in NhaA on activation and during transport, which includes changes in the conformation of TM 4.[48,57] Thus, it may also be important that the interaction between TM VI and VII is weak to allow for these conformational changes, as well.

In conclusion, we successfully expressed and determined the structure of a two-transmembrane segment of the Na^+/H^+ exchanger, NHE1. The structure of TM VI–VII in DPC micelles consists of two helices separated by an extended region in TM VI, and a straight helix in TM VII, with TM VI and TM VII interacting around the connecting interhelical loop. A resemblance of TM VI–VII of NHE1 to TM 4–5 of NhaA suggests that these two regions share the same structure and function in the full length protein. The proposed interaction between TM VI and TM VII is supported by Trp scanning mutagenesis, which showed that insertion of a bulky Trp residue into the region of amino acids 240–245 disrupted NHE1 activity. Our study holds promise for determining the structures of further pairs of TM segments or larger transmembrane segments, to assemble the structure of the entire protein.

■ ASSOCIATED CONTENT

Supporting Information

Oligonucleotides used for site-directed mutagenesis and comparison of NMR relaxation data. This material is available free of charge via the Internet at http://pubs.acs.org.

■ AUTHOR INFORMATION

Corresponding Author

*Department of Biochemistry, 347 Medical Science Building, University of Alberta, Edmonton, Alberta, Canada T6G 2H7. E-mail: lfliegel@ualberta.ca. Phone: (780) 492-1848. Fax: (780) 492-0886.

Author Contributions

C.A. and B.L.L. contributed equally to this work.

Funding

Funded by the Canadian Institute of Health Research. C.A. was partially supported by a one-year CNPq fellowship, Brazil. B.L.L. was supported by Alberta Innovates Health Solutions and the Heart and Stroke Foundation of Canada.

Notes

The authors declare no competing financial interest.

■ ACKNOWLEDGMENTS

We thank the Canadian National High Field NMR Centre for assistance with and use of the 800 MHz spectrometer.

■ ABBREVIATIONS

DPC, dodecylphosphocholine; HA, hemagglutinin; pH_i, intracellular pH; MBP, maltose binding protein; NHE1, Na^+/H^+ exchanger isoform 1; NMR, nuclear magnetic resonance; TEV, tobacco etch virus; TM, transmembrane.

■ REFERENCES

(1) Karmazyn, M., Sawyer, M., and Fliegel, L. (2005) The Na^+/H^+ exchanger: A target for cardiac therapeutic intervention. *Curr. Drug Targets: Cardiovasc. & Haematol. Disord. 5*, 323–335.

(2) Fliegel, L. (2009) Regulation of the Na^+/H^+ exchanger in the healthy and diseased myocardium. *Expert Opin. Ther. Targets 13*, 55–68.

(3) Harris, C., and Fliegel, L. (1999) Amiloride and the Na^+/H^+ exchanger protein. Mechanism and significance of inhibition of the Na^+/H^+ exchanger. *Int. J. Mol. Med. 3*, 315–321.

(4) Grinstein, S., Rotin, D., and Mason, M. J. (1989) Na^+/H^+ exchange and growth factor-induced cytosolic pH changes. Role in cellular proliferation. *Biochim. Biophys. Acta 988*, 73–97.

(5) Shrode, L., Cabado, A., Goss, G., and Grinstein, S. (1996) Role of the Na^+/H^+ antiporter isoforms in cell volume regulation. In *The Na^+/H^+ Exchanger* (Fliegel, L., Ed.) 101–122, R. G. Landes Co., Austin, TX.

(6) Denker, S. P., and Barber, D. L. (2002) Cell migration requires both ion translocation and cytoskeletal anchoring by the Na-H exchanger NHE1. *J. Cell Biol. 159*, 1087–1096.

(7) Busco, G., Cardone, R. A., Greco, M. R., Bellizzi, A., Colella, M., Antelmi, E., Mancini, M. T., Dell'Aquila, M. E., Casavola, V., Paradiso, A., and Reshkin, S. J. (2010) NHE1 promotes invadopodial ECM proteolysis through acidification of the peri-invadopodial space. *FASEB J. 24*, 3903–3915.

(8) Stock, C., Cardone, R. A., Busco, G., Krahling, H., Schwab, A., and Reshkin, S. J. (2008) Protons extruded by NHE1: Digestive or glue? *Eur. J. Cell Biol. 87*, 591–599.

(9) Harguindey, S., Orive, G., Luis Pedraz, J., Paradiso, A., and Reshkin, S. J. (2005) The role of pH dynamics and the Na^+/H^+ antiporter in the etiopathogenesis and treatment of cancer. Two faces of the same coin—one single nature. *Biochim. Biophys. Acta 1756*, 1–24.

(10) Paradiso, A., Cardone, R. A., Bellizzi, A., Bagorda, A., Guerra, L., Tommasino, M., Casavola, V., and Reshkin, S. J. (2004) The Na^+-H^+ exchanger-1 induces cytoskeletal changes involving reciprocal RhoA and Rac1 signaling, resulting in motility and invasion in MDA-MB-435 cells. *Breast Cancer Res. 6*, R616–R628.

(11) Amith, S. R., and Fliegel, L. (2013) Regulation of the Na^+/H^+ Exchanger (NHE1) in Breast Cancer Metastasis. *Cancer Res. 73*, 1259−1264.
(12) Fliegel, L., Dyck, J. R. B., Wang, H., Fong, C., and Haworth, R. S. (1993) Cloning and analysis of the human myocardial Na^+/H^+ exchanger. *Mol. Cell. Biochem. 125*, 137−143.
(13) Mraiche, F., Oka, T., Gan, X. T., Karmazyn, M., and Fliegel, L. (2011) Activated NHE1 is required to induce early cardiac hypertrophy in mice. *Basic Res. Cardiol. 106*, 603−616.
(14) Karmazyn, M., Liu, Q., Gan, X. T., Brix, B. J., and Fliegel, L. (2003) Aldosterone increases NHE-1 expression and induces NHE-1-dependent hypertrophy in neonatal rat ventricular myocytes. *Hypertension 42*, 1171−1176.
(15) Fliegel, L. (2008) Molecular biology of the myocardial Na^+/H^+ exchanger. *J. Mol. Cell. Cardiol. 44*, 228−237.
(16) Murphy, E., and Allen, D. G. (2009) Why did the NHE inhibitor clinical trials fail? *J. Mol. Cell. Cardiol. 46*, 137−141.
(17) Wakabayashi, S., Pang, T., Su, X., and Shigekawa, M. (2000) A novel topology model of the human Na^+/H^+ exchanger isoform 1. *J. Biol. Chem. 275*, 7942−7949.
(18) Landau, M., Herz, K., Padan, E., and Ben-Tal, N. (2007) Model structure of the Na^+/H^+ exchanger 1 (NHE1): Functional and clinical implications. *J. Biol. Chem. 282*, 37854−37863.
(19) Kemp, G., Young, H., and Fliegel, L. (2008) Structure and function of the human Na^+/H^+ exchanger isoform 1. *Channels 2*, 329−336.
(20) Cunningham, F., and Deber, C. M. (2007) Optimizing synthesis and expression of transmembrane peptides and proteins. *Methods 41*, 370−380.
(21) Hunt, J. F., Earnest, T. N., Bousche, O., Kalghatgi, K., Reilly, K., Horvath, C., Rothschild, K. J., and Engelman, D. M. (1997) A biophysical study of integral membrane protein folding. *Biochemistry 36*, 15156−15176.
(22) Katragadda, M., Alderfer, J. L., and Yeagle, P. L. (2001) Assembly of a polytopic membrane protein structure from the solution structures of overlapping peptide fragments of bacteriorhodopsin. *Biophys. J. 81*, 1029−1036.
(23) Tzeng, J., Lee, B. L., Sykes, B. D., and Fliegel, L. (2010) Structural and functional analysis of transmembrane segment VI of the NHE1 isoform of the Na^+/H^+ exchanger. *J. Biol. Chem. 285*, 36656−36665.
(24) Tzeng, J., Lee, B. L., Sykes, B. D., and Fliegel, L. (2011) Structural and functional analysis of critical amino acids in TM VI of the NHE1 isoform of the Na^+/H^+ exchanger. *Biochim. Biophys. Acta 1808*, 2327−2335.
(25) Ding, J., Ng, R. W. P., and Fliegel, L. (2007) Functional characterization of the transmembrane segment VII of the NHE1 isoform of the Na^+/H^+ exchanger. *Can. J. Physiol. Pharmacol. 85*, 319−325.
(26) Ding, J., Rainey, J. K., Xu, C., Sykes, B. D., and Fliegel, L. (2006) Structural and functional characterization of transmembrane segment VII of the Na^+/H^+ exchanger isoform 1. *J. Biol. Chem. 281*, 29817−29829.
(27) Douglas, J. L., Trieber, C. A., Afara, M., and Young, H. S. (2005) Rapid, high-yield expression and purification of Ca^{2+}-ATPase regulatory proteins for high-resolution structural studies. *Protein Expression Purif. 40*, 118−125.
(28) Slepkov, E. R., Rainey, J. K., Li, X., Liu, Y., Cheng, F. J., Lindhout, D. A., Sykes, B. D., and Fliegel, L. (2005) Structural and functional characterization of transmembrane segment IV of the NHE1 isoform of the Na^+/H^+ exchanger. *J. Biol. Chem. 280*, 17863−17872.
(29) Schagger, H. (2006) Tricine-SDS-PAGE. *Nat. Protoc. 1*, 16−22.
(30) Delaglio, F., Grzesiek, S., Vuister, G. W., Zhu, G., Pfeifer, J., and Bax, A. (1995) NMRPipe: A multidimensional spectral processing system based on UNIX pipes. *J. Biomol. NMR 6*, 277−293.
(31) Johnson, B. A., and Blevins, R. A. (1994) NMRView: A computer program for the visualization and analysis of NMR data. *J. Biomol. NMR 4*, 603−614.
(32) Wuthrich, K. (1986) *NMR of proteins and nucleic acids*, Wiley, New York.
(33) Wishart, D. S., Sykes, B. D., and Richards, F. M. (1992) The chemical shift index: A fast and simple method for the assignment of protein secondary structure through NMR spectroscopy. *Biochemistry 31*, 1647−1651.
(34) Rainey, J. K., Fliegel, L., and Sykes, B. D. (2006) Strategies for dealing with conformational sampling in structural calculations of flexible or kinked transmembrane peptides. *Biochem. Cell Biol. 84*, 918−929.
(35) Schwieters, C. D., Kuszewski, J. J., Tjandra, N., and Clore, G. M. (2003) The Xplor-NIH NMR molecular structure determination package. *J. Magn. Reson. 160*, 65−73.
(36) Slepkov, E. R., Chow, S., Lemieux, M. J., and Fliegel, L. (2004) Proline residues in transmembrane segment IV are critical for activity, expression and targeting of the Na^+/H^+ exchanger isoform 1. *Biochem. J. 379*, 31−38.
(37) Moor, A., Gan, X. T., Karmazyn, M., and Fliegel, L. (2001) Activation of Na^+/H^+ exchanger-directed protein kinases in the ischemic and ischemic-reperfused rat myocardium. *J. Biol. Chem. 27*, 16113−16122.
(38) Wang, H., Singh, D., and Fliegel, L. (1997) The Na^+/H^+ antiporter potentiates growth and retinoic-acid induced differentiation of P19 embryonal carcinoma cells. *J. Biol. Chem. 272*, 26545−26549.
(39) Schushan, M., Landau, M., Padan, E., and Ben-Tal, N. (2011) Two Conflicting NHE1 Model Structures: Compatibility with Experimental Data and Implications for the Transport Mechanism. *J. Biol. Chem. 286*, le9.
(40) Ullah, A., Kemp, G., Lee, B., Alves, C., Young, H., Sykes, B. D., and Fliegel, L. (2013) Structural and Functional Analysis of Transmembrane Segment IV of the Salt Tolerance Protein Sod2. *J. Biol. Chem. 288*, 24609−24624.
(41) Reddy, T., Li, X., Fliegel, L., Sykes, B. D., and Rainey, J. K. (2010) Correlating structure, dynamics, and function in transmembrane segment VII of the Na^+/H^+ exchanger isoform 1. *Biochim. Biophys. Acta 1798*, 94−104.
(42) Hutchinson, E. G., and Thornton, J. M. (1996) PROMOTIF: A program to identify and analyze structural motifs in proteins. *Protein Sci. 5*, 212−220.
(43) Lee, B. L., Li, X., Liu, Y., Sykes, B. D., and Fliegel, L. (2009) Structural and functional analysis of transmembrane XI of the NHE1 isoform of the Na^+/H^+ exchanger. *J. Biol. Chem. 284*, 11546−11556.
(44) Reddy, T., Ding, J., Li, X., Sykes, B. D., Rainey, J. K., and Fliegel, L. (2008) Structural and functional characterization of transmembrane segment IX of the NHE1 isoform of the Na^+/H^+ exchanger. *J. Biol. Chem. 283*, 22018−22030.
(45) Lee, B. L., Sykes, B. D., and Fliegel, L. (2013) Structural and functional insights into the cardiac Na^+/H^+ exchanger. *J. Mol. Cell. Cardiol. 61*, 60−67.
(46) Lee, B. L., Sykes, B. D., and Fliegel, L. (2011) Structural analysis of the Na^+/H^+ exchanger isoform 1 (NHE1) using the divide and conquer approach. *Biochem. Cell Biol. 89*, 189−199.
(47) Rimon, A., Kozachkov-Magrisso, L., and Padan, E. (2012) The unwound portion dividing helix IV of NhaA undergoes a conformational change at physiological pH and lines the cation passage. *Biochemistry 51*, 9560−9569.
(48) Arkin, I. T., Xu, H., Jensen, M. O., Arbely, E., Bennett, E. R., Bowers, K. J., Chow, E., Dror, R. O., Eastwood, M. P., Flitman-Tene, R., Gregersen, B. A., Klepeis, J. L., Kolossvary, I., Shan, Y., and Shaw, D. E. (2007) Mechanism of Na^+/H^+ antiporting. *Science 317*, 799−803.
(49) Goswami, P., Paulino, C., Hizlan, D., Vonck, J., Yildiz, O., and Kuhlbrandt, W. (2011) Structure of the archaeal Na^+/H^+ antiporter NhaP1 and functional role of transmembrane helix 1. *EMBO J. 30*, 439−449.
(50) Hu, N. J., Iwata, S., Cameron, A. D., and Drew, D. (2011) Crystal structure of a bacterial homologue of the bile acid sodium symporter ASBT. *Nature 478*, 408−411.

(51) Lee, C., Kang, H. J., von Ballmoos, C., Newstead, S., Uzdavinys, P., Dotson, D. L., Iwata, S., Beckstein, O., Cameron, A. D., and Drew, D. (2013) A two-domain elevator mechanism for sodium/proton antiport. *Nature 501*, 573−577.
(52) Salussolia, C. L., Corrales, A., Talukder, I., Kazi, R., Akgul, G., Bowen, M., and Wollmuth, L. P. (2011) Interaction of the M4 Segment with Other Transmembrane Segments Is Required for Surface Expression of Mammalian α-Amino-3-hydroxy-5-methyl-4-isoxazolepropionic Acid (AMPA) Receptors. *J. Biol. Chem. 286*, 40205−40218.
(53) Santiago, J., Guzman, G. R., Torruellas, K., Rojas, L. V., and Lasalde-Dominicci, J. A. (2004) Tryptophan scanning mutagenesis in the TM3 domain of the *Torpedo californica* acetylcholine receptor β subunit reveals an α-helical structure. *Biochemistry 43*, 10064−10070.
(54) Otero-Cruz, J. D., Baez-Pagan, C. A., Caraballo-Gonzalez, I. M., and Lasalde-Dominicci, J. A. (2007) Tryptophan-scanning mutagenesis in the αM3 transmembrane domain of the muscle-type acetylcholine receptor. A spring model revealed. *J. Biol. Chem. 282*, 9162−9171.
(55) Irizarry, S. N., Kutluay, E., Drews, G., Hart, S. J., and Heginbotham, L. (2002) Opening the KcsA K^+ channel: Tryptophan scanning and complementation analysis lead to mutants with altered gating. *Biochemistry 41*, 13653−13662.
(56) Hunte, C., Screpanti, E., Venturi, M., Rimon, A., Padan, E., and Michel, H. (2005) Structure of a Na^+/H^+ antiporter and insights into mechanism of action and regulation by pH. *Nature 435*, 1197−1202.
(57) Appel, M., Hizlan, D., Vinothkumar, K. R., Ziegler, C., and Kuhlbrandt, W. (2009) Conformations of NhaA, the Na^+/H^+ exchanger from *Escherichia coli*, in the pH-activated and ion-translocating states. *J. Mol. Biol. 388*, 659−672.
(58) Laskowski, R. A., Rullmannn, J. A., MacArthur, M. W., Kaptein, R., and Thornton, J. M. (1996) AQUA and PROCHECK-NMR: Programs for checking the quality of protein structures solved by NMR. *J. Biomol. NMR 8*, 477−486.
(59) Guntert, P. (2004) Automated NMR structure calculation with CYANA. *Methods Mol. Biol. 278*, 353−378.